NANO LETTERS

pubs.acs.org/NanoLett Letter

Electrolyte Anion-Initiated In Situ Polymerization of Dioxolane-Derived Gel Electrolytes for Dendrite-Resistant and Separator-Free Lithium Metal Batteries

Tianyu Shen, Qianchuan Yu, Jie Wei, Yaoda Wang, Huaizhu Wang, Zhenchao Li, Xingkai Ma, Jingjie Sun, Jing Ma, Zuoxiu Tie,* and Zhong Jin*

Cite This: *Nano Lett.* 2025, 25, 10102−10113 Read Online

ACCESS | Metrics & More | Article Recommendations | Supporting Information

ABSTRACT: The practicality of solid-state lithium metal batteries is limited by poor interfacial contact and low ion conductivity of solid-state electrolytes. Herein, we report a gel polymer electrolyte composed of $LiN(SO_2F)_2$ and polymerized dioxolane prepared via in situ ring-opening polymerization triggered by radicals without the need for additional initiators and separators. Theoretical and experimental studies revealed a polymerization mechanism involving S−F bond rupture in $LiN(SO_2F)_2$, followed by attack of a Lewis-acidic S atom in the $\bullet(SO_2)(FSO_2)N^-$ radical on a Lewis-basic O atom in dioxolane. The electrolyte demonstrated high ion conductivity (1.836 mS cm^{-1}) and Li-ion transference number (0.705), significantly improving the Li plating/stripping uniformity and long-term stability. Batteries with such electrolytes exhibited high-rate capability, high Coulombic efficiency, high capacity retention (75.1% after 3000 cycles), and broad temperature tolerance (−15 to 70 °C). Our research underscores the potential of in situ polymerization in fabricating gel polymer electrolytes to promote the development of secondary alkali metal batteries with exceptional energy density and stability.

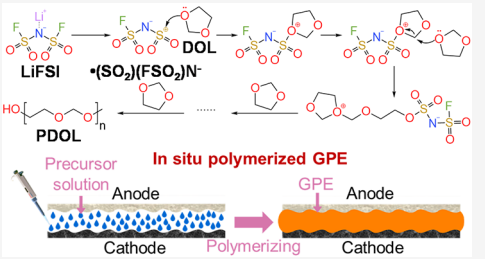

KEYWORDS: *Solid-state lithium metal batteries, Gel polymer electrolytes, Radical trigged ring-opening polymerization, Wide temperature range, Lithium dendrite suppression*

The development of high-specific-energy lithium metal batteries (LMBs) is hindered by poor electrochemical stability, high flammability, and side reactions of traditional liquid organic electrolytes (LOEs).[1−11] Currently, organic polymer-based solid-state electrolytes, also known as gel polymer electrolytes (GPEs), have garnered significant interest due to their commendable ion conductivity, exceptional mechanical resilience, and economical production costs.[12−29] Particularly, polymerized dioxolane (PDOL)-based GPEs have exhibited high ion conductivity and high Li-ion transference number (t_{Li}^+).[30−37] Nevertheless, there are some concerns arising from the employment of PDOL-based GPEs. First, the polymerization process necessitates additional initiators that unfortunately exert detrimental impacts on the overall battery performances, as evidenced in prior studies.[6−10] Second, despite advancements, the need for separators to prevent short circuits and ensure safety remains.[6−9,35]

Herein, we introduce an innovative GPE prepared via $LiN(SO_2F)_2$ (LiFSI)-triggered in situ ring-opening polymerization (ROP) of DOL, namely LiFSI/PDOL GPE, which uniquely eliminates the necessity of additional polymerization initiators and separators. Comparative experiments and theoretical calculations were conducted to explore the mechanism of radical-initiated ROP, revealing a detailed reaction process involving the break of S−F bonds in LiFSI followed by attack of a Lewis-acidic S atom in a $\bullet(SO_2)(FSO_2)N^-$ radical on a Lewis-basic O atom in DOL. The improved polymerization procedure enables such GPE to combine several advantages of high ion conductivity (1.836 mS cm^{-1}), high t_{Li}^+ (0.705), thin thickness (80 μm), and low production costs. Moreover, the in situ polymerization strategy ensures sufficient contact between the electrode and electrolyte, leading to ultralow interfacial resistance and fast Li-ion mass-transfer kinetics. The favorable solid-electrolyte interphase (SEI) generated by LiFSI/PDOL GPE can significantly improve the uniformity and long-term stability of Li plating/stripping processes. Characterizations verified that LiF-containing SEI resulted from LiFSI decomposition is conducive to uniform Li deposition and inhibits lithium-dendrite growth. Therefore, Li||LiFSI/PDOL GPE||Li symmetric batteries maintained stable and dendrite-free cycling for over 500 h at 1.0 mA cm^{-2}. Li||LiFSI/PDOL GPE||$LiFePO_4$

Received: April 4, 2025
Revised: May 31, 2025
Accepted: June 4, 2025
Published: June 10, 2025

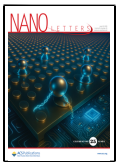

https://doi.org/10.1021/acs.nanolett.5c01953
Nano Lett. 2025, 25, 10102−10113

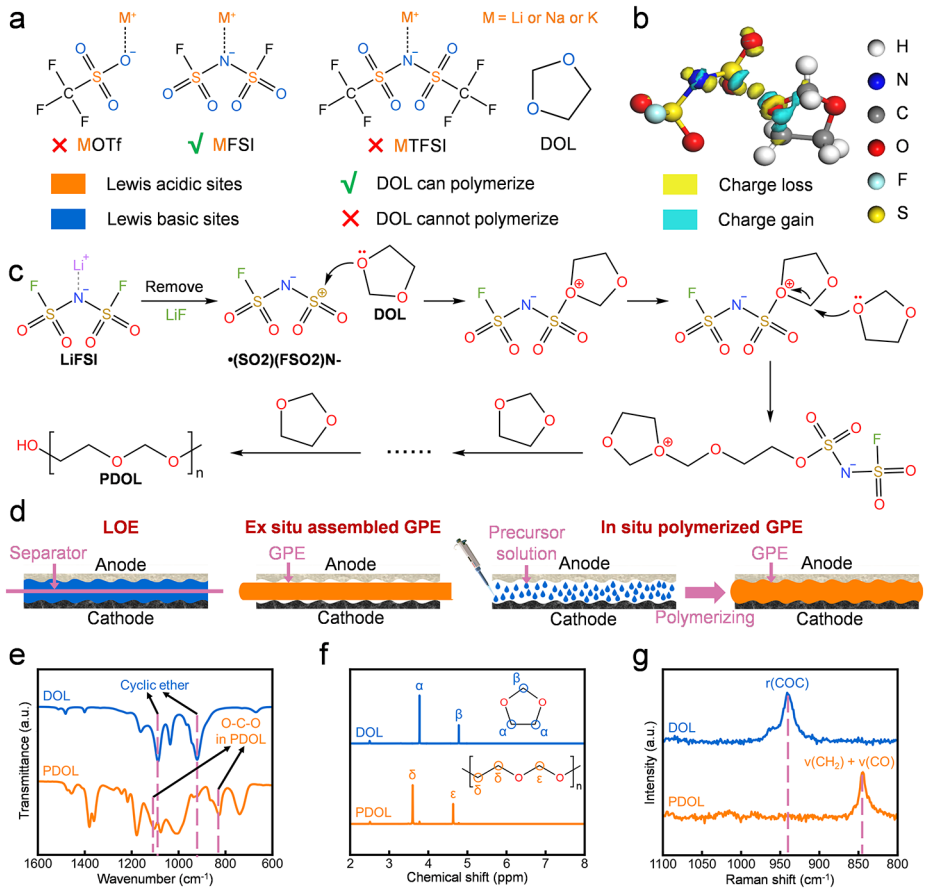

Figure 1. Mechanism study and characterization. (a) Lewis acid/base sites of different lithium salts and DOL. (b) DCD diagram of interaction between $\bullet(SO_2)(FSO_2)N^-$ and DOL. (c) The reaction mechanism of ROP of DOL trigged by $\bullet(SO_2)(FSO_2)N^-$. (d) Schematic illustration of batteries assembled with LOE, ex situ assembled GPE, and in situ polymerized GPE. (e) ATR-FTIR, (f) ^{1}H NMR, and (g) Raman spectra of DOL before and after ROP.

(LFP) batteries showed a high Coulombic efficiency (CE, 99.8%) and a high capacity-retention capability (75.1%) after 3000 cycles at 1.0 C. Thanks to the broad electrochemical window of LiFSI/PDOL GPE, the as-fabricated Lill $LiNi_{0.8}Co_{0.1}Mn_{0.1}O_2$ (NCM811) batteries also displayed excellent cycling stability and high remaining capacity (132.06 mAh g^{-1}) after 350 cycles. Moreover, LMBs with LiFSI/PDOL GPE functioned stably at extreme temperatures (70 and −15 °C), showcasing considerable potential for widespread use under diverse regional and climate conditions. This study highlights the tremendous potential of the in situ polymerization strategy in enhancing the stability and lifespan and improving the operating temperature of rechargeable alkali metal batteries.

To investigate the reaction mechanism of the LiFSI-initiated ROP of DOL, a series of comparative experiments were conducted. The results showed that ROP of DOL initiated by LiFSI is closely related to FSI^-, while Li^+ does not play a central role in initiation process (Figure S1). ROP of DOL requires a Lewis-acidic site to react with a lone-electron pair on O in DOL.[6−10] As illustrated in Figure 1a, only S in FSI^- possesses Lewis acidity, while N and O have Lewis alkalinity. To further explore the mechanism, a theoretical calculation was employed. A differential charge density (DCD) diagram (Figure 1b) indicated a strong interaction between S in $\bullet(SO_2)(FSO_2)N^-$ and O in DOL, suggesting high reactivity between two species. Additionally, changes in charge density of DOL lead to the weakening or strengthening of corresponding bonds, as quantified by bond-length analysis (Figure S2). Further calculations (Figures S3, S4) excluded the possibility of FSI^-, FSO_2N, $TFSI^-$, and OTf^- initiating DOL polymerization. These findings supported the mechanism of FSI^--initiated DOL ROP, indicating that the electron-deficient S center of $\bullet(SO_2)(FSO_2)N^-$ triggers the polymerization reaction.

Based on these experimental and theoretical results, a plausible reaction mechanism for radical-triggered DOL ROP was proposed (Figure 1c). The Li ion in LiFSI coordinates with Lewis-basic O in the FSI^- sulfonyl group, reducing the electronic density around the sulfonyl group and weakening the S−F bond. This leads to S−F bond breaking and the formation of stable LiF, confirmed by the X-ray diffraction spectrum of as-prepared PDOL (Figure S5). Although the cleavage of the S−F bond requires overcoming its bond energy (normally ∼327 kJ mol^{-1}), the coordination effect in LiFSI/PDOL GPE greatly reduced this value to 124.14 kJ mol^{-1} (Figure S6), indicating that S−F bond cleavage is thermodynamically favorable in our system. After the S−F bond breaks, the Lewis acidity of S in $\bullet(SO_2)(FSO_2)N^-$ is significantly enhanced, forming an electron-deficient S center, further confirmed by electron paramagnetic resonance spectrum of PDOL (Figure S7). Subsequently, O in DOL is attacked by Lewis-acidic S, with lone-pair electrons of O sharing with the empty orbital of S to form the onium ion. The positive center

https://doi.org/10.1021/acs.nanolett.5c01953
Nano Lett. 2025, 25, 10102−10113

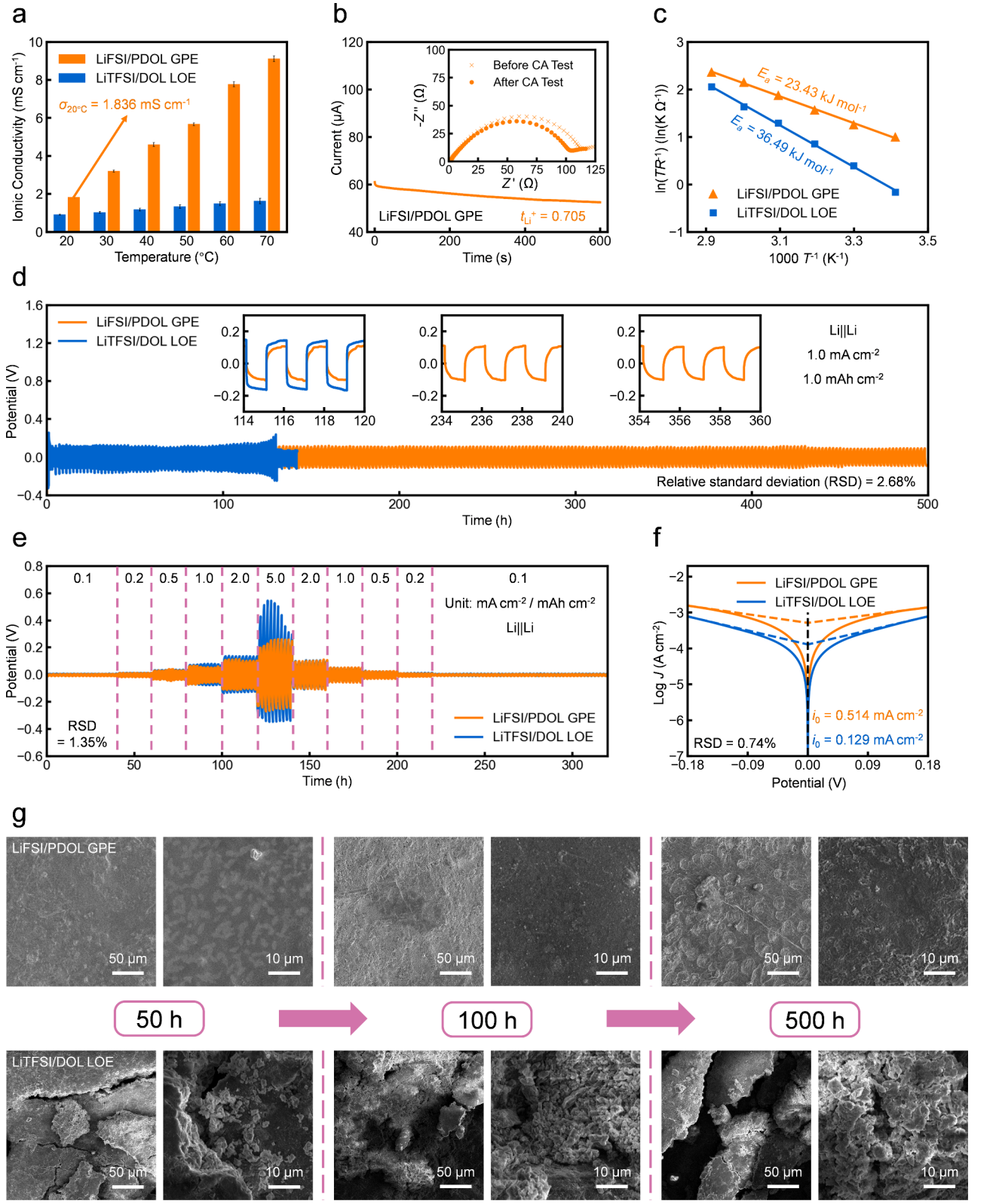

Figure 2. Electrochemical performances. (a) Ion conductivities, (b) t_{Li}^{+}, and (c) activation energy of LiFSI/PDOL GPE and LiTFSI/DOL LOE. (d) Galvanostatic cycling stability, (e) rate performance, and (f) Tafel curves of Li||Li symmetric batteries. (g) SEM images of Li electrodes retrieved from Li||Li batteries after Li plating/stripping cycling.

then transfers from S to O, initiating the subsequent ROP of DOL. Theoretical calculations confirmed that only the electron-deficient S center in $\bullet(SO_2)(FSO_2)N^-$ can initiate ROP of DOL, verifying the proposed mechanism (Figure 1c).

In addition to the reaction mechanism, an innovative in situ synthetic route for LiFSI/PDOL GPE was developed using radical-triggered ROP of DOL with LiFSI as the sole initiator. This in situ preparation allows for sufficient contact between

https://doi.org/10.1021/acs.nanolett.5c01953
Nano Lett. 2025, 25, 10102−10113

the electrode and electrolyte, resulting in a significant decrease in interface impedance (Figure 1d). Notably, LiFSI/PDOL GPE can be manufactured by a one-step casting method without additional additives, simplifying the battery manufacturing process and reducing production costs. Conversely, traditional LOEs are prone to leaking and require separators which are inconvenient and expensive. Ex situ assembled GPEs usually lead to poor contact between electrodes and electrolytes, resulting in high interface resistances.

Various spectroscopic techniques were employed to analyze the LiFSI/PDOL GPE prepared via this method. The attenuated total reflectance Fourier transform infrared (ATR-FTIR) spectra (Figure 1e) demonstrated the appearance of new characteristic peaks representing O−C−O chain in PDOL at 1103 and 827 cm^{-1} and the disappearance of peaks representing the cyclic ether in DOL at 921 and 1090 cm^{-1}, indicating successful DOL polymerization.[6,7,15] The ^1H nuclear magnetic resonance (NMR) spectra (Figure 1f) reveal the disappearance of chemical shifts associated with DOL at 3.77 and 4.78 ppm. Meanwhile, new peaks attributed to H elements in PDOL appear at 3.60 and 4.63 ppm, and the integral area ratio of these peaks is consistent to the quantitative ratio of distinct H elements in DOL or PDOL, further confirming successful DOL polymerization.[6,7] Finally, Raman spectra (Figure 1g) reveal the disappearance of a DOL-related peak (844 cm^{-1}, associated with the −C−O−C− ring stretching) and the appearance of a PDOL-related peak (941 cm^{-1}, attributed to the vibration of −C−O− and $-CH_2-$), providing additional evidence of DOL polymerization.[6]

Optical and scanning electron microscope (SEM) images of LiFSI/PDOL GPE (Figures S8−S10) presented a transparent gel shape and a smooth and dense surface, with a thickness of approximately 80 μm. This precise thickness control was achieved by adjusting the precursor solution volume (40 μL cm^{-2} yielding 80 μm) with a linear correlation between the solution volume and membrane thickness, verified via SEM and thickness gauge measurements. Thermogravimetric analysis (Figure S11) identified the compositions of LiFSI/PDOL GPE, revealing its PDOL content (36.96 wt %). Overall, these results confirmed that LiFSI can successfully initiate ROP of DOL, making the LiFSI/PDOL GPE a promising candidate for high-performance and cost-effective solid-state LMBs (SSLMBs).

To further evaluate the electrochemical properties of LiFSI/PDOL GPE, stainless-steel (SS)||SS and Li||Li symmetrical batteries were assembled for testing, with a traditional LiTFSI/DOL LOE serving as a control. Ion-conductivity measurements (Figure S12 and Tables S1 and S2) revealed that LiFSI/PDOL GPE exhibits a higher ion conductivity comparable to LiTFSI/DOL LOE at various temperatures (20 to 70 °C), with a room-temperature value of approximately 1.836 mS cm^{-1} (Figure 2a), surpassing most previously reported GPEs (Table S5). The t_{Li}^+ of LiFSI/PDOL GPE showed a high value of 0.705 (Figure 2b), significantly greater than that of LiTFSI/DOL LOE (0.326, Figure S13). The activation energies (E_a) for Li-ion transport in LiFSI/PDOL GPE and LiTFSI/DOL LOE were calculated to be 23.43 and 36.49 kJ mol^{-1}, respectively (Figure 2c, Figure S14, and Tables S3 and S4), indicating that LiFSI/PDOL GPE has lower activation energy, demonstrating excellent Li-ion transfer capability and low interface impedance due to sufficient electrode/electrolyte contact through the in situ strategy.

Molecular dynamics (MD) simulations were performed to reveal the distinct solvation structures underlying these performance differences (Figure S15). In LiTFSI/DOL LOE, Li^+ is predominantly coordinated by $TFSI^-$ (Li^+-$TFSI^-$ coordination number ≈ 3.2) with the partial participation of DOL oxygen atoms, forming a relatively rigid solvation structure that impedes rapid Li^+ migration. Conversely, the LiFSI/PDOL GPE exhibits a more dissociated ionic environment. The FSI^- demonstrates weaker coordination (Li^+-FSI^- coordination number ≈ 2.1) due to steric effects from the PDOL polymer matrix, which preferentially interacts with Li^+ through ether oxygen sites. This weakened solvation reduces the activation energy for Li^+ desolvation ($\Delta E_{desolvation}$ = 3.74 eV for LiFSI/PDOL GPE vs 4.57 eV for LiTFSI/DOL LOE) and increases the Li^+ diffusion coefficient, as quantified by the mean square displacement analysis (Figure S16). Furthermore, the immobilized PDOL chains restrict anion (FSI^-) mobility while maintaining Li^+ conduction pathways, elevating t_{Li}^+ from 0.33 (LiTFSI/DOL LOE) to 0.71 (LiFSI/PDOL GPE). The synergy of all these effects—optimized solvation structure, reduced desolvation barriers, and selective ion transport—leads to the superior ionic transport properties of LiFSI/PDOL GPE, well aligning with our experimental results.

Galvanostatic charge/discharge tests of Li||Li batteries were conducted to evaluate the electrochemical kinetics and long-term stability of LiFSI/PDOL GPE. The Li||LiFSI/PDOL GPE||Li battery remained stable for 500 h, with an overpotential below 120 mV and no voltage polarization at 1.0 mA cm^{-2} and 1.0 mAh cm^{-2} (Figure 2d), suggesting a very stable Li-ion plating/stripping behavior. Conversely, the Li||LiTFSI/DOL LOE||Li battery showed higher overpotential with a voltage polarization after 100 h and a short-circuit occurring after 130 h due to Li dendrite penetration, indicating its uneven Li-ion plating/stripping behavior. A similar test at 0.5 mA cm^{-2} and 0.5 mAh cm^{-2} for the Li||LiFSI/PDOL GPE||Li battery maintained an overpotential below 60 mV for 1000 h (Figure S17), while the Li||LiTFSI/DOL LOE||Li battery experienced a short circuit within 200 h. These results demonstrated the excellent Li-ion transfer kinetics and long-term stability of LiFSI/PDOL GPE. Rate performances were evaluated at various current densities (0.1 to 5.0 mA cm^{-2}), showing limited voltage polarizations of the Li||LiFSI/PDOL GPE||Li battery (Figure 2e), significantly lower than the Li||LiTFSI/DOL LOE||Li battery (Figure S18). Tafel plots (Figure 2f) revealed exchange current densities (i_0) of 0.514 and 0.129 mA cm^{-2} for LiFSI/PDOL GPE and LiTFSI/DOL LOE, respectively, further supporting the superior charge-transfer kinetics of the LiFSI/PDOL GPE.

SEM images of Li electroplating morphology after cycling (Figure 2g) showed that LiFSI/PDOL GPE achieved stable Li-ion plating/stripping with flat surfaces and slight protrusions even after 500 h, confirming its ability of inhibiting lithium-dendrite growth. Conversely, Li electrodes cycled in LiTFSI/DOL LOE exhibited cracks, rough surfaces, and severe lithium-dendrite growth after 50 h, with complete coverage by blocky dead Li and numerous cracks after 500 h.

Overall, LiFSI/PDOL GPE outperforms LiTFSI/DOL LOE in ion conductivity, t_{Li}^+, interface impedance, and cycle stability, attributed to ample Li-ion transmission channels, optimized solvation structure, reduced desolvation barriers, enhanced mechanical strength, good wettability, and optimized SEI-layer compositions.[2,6−10,38]

https://doi.org/10.1021/acs.nanolett.5c01953
Nano Lett. 2025, 25, 10102−10113

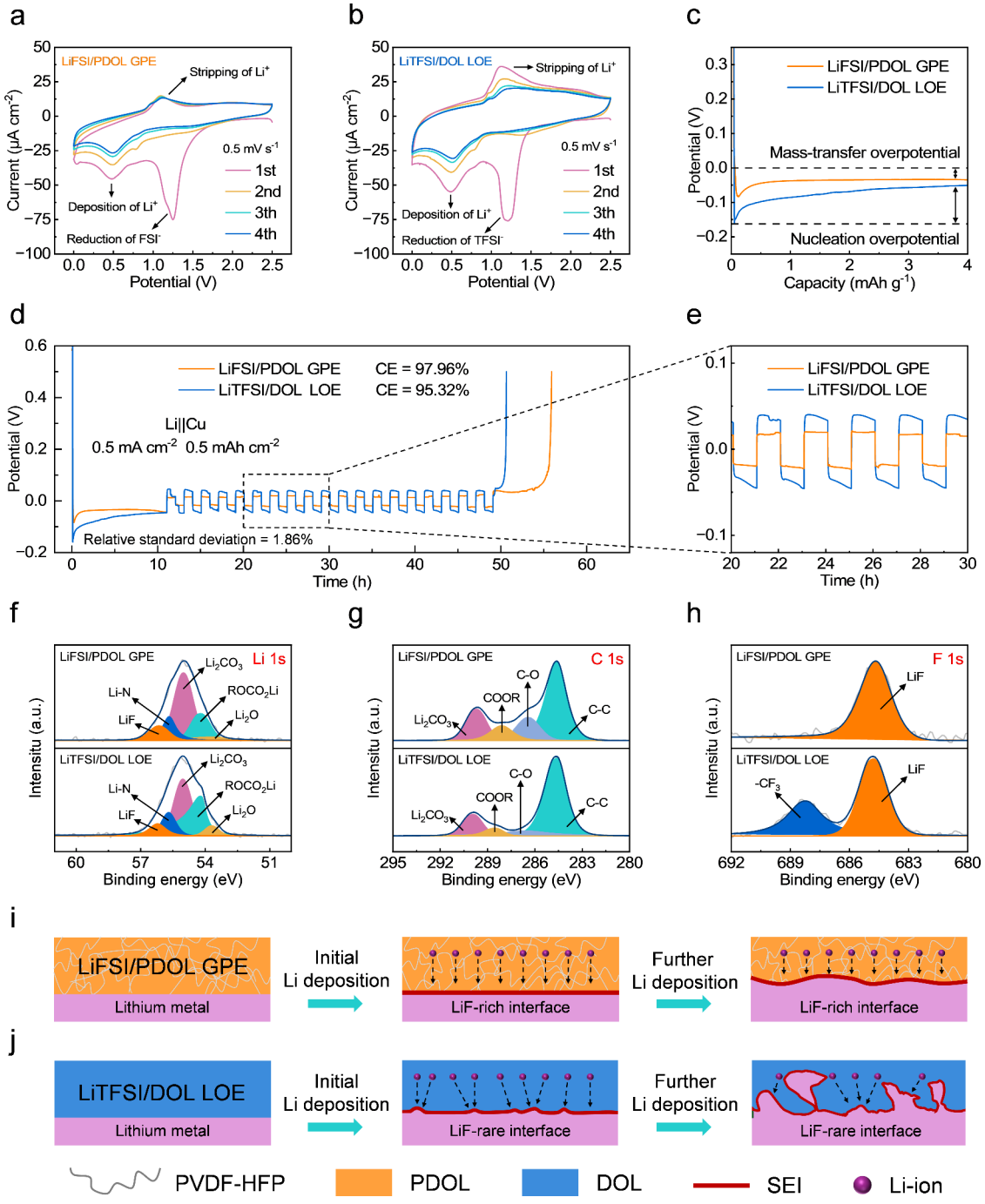

Figure 3. Lithium deposition behaviors. CV curves of Li||Cu half batteries assembled with (a) LiFSI/PDOL GPE or (b) LiTFSI/DOL LOE. (c) Voltage profiles during the initial Li deposition process and (d, e) voltage−time curves of Li||Cu half batteries. (f−h) XPS spectra of Li electrodes retrieved from Li||Li batteries. (i, j) Schematic illustrations of Li plating/stripping behaviors.

To investigate the evolution and compositional differences of the SEI layer on lithium anodes using LiFSI/PDOL GPE or LiTFSI/DOL LOE, cyclic voltammetry (CV) was performed on Li||Cu half batteries. During the first discharge cycle, reduction peaks appeared at 0.50 V (lithium deposition on Cu) and 1.25 V (redox decomposition of FSI^- or TFSI), indicating SEI-layer formation from electrolyte decomposition (Figure 3a, b). To assess the impact of the SEI layer on lithium plating/stripping processes, Li-utilization efficiency was measured using Aurbach's methodology (Figure 3d).[39] Li||Cu batteries with LiFSI/PDOL GPE showed a higher average CE (97.96%) compared to LiTFSI/DOL LOE (95.32%). Additionally, Li||LiFSI/PDOL GPE||Cu batteries demonstrated reduced voltage polarization, underscoring its enhanced Li-ion mass-transfer kinetics (Figure 3e). Nucleation and mass-transfer overpotentials during initial lithium deposition stages revealed lower values of 49.9 and 33.6 mV for LiFSI/PDOL GPE versus 107.5 and 51.8 mV for LiTFSI/DOL LOE (Figure 3c and Figure S19), suggesting that the SEI layer generated via FSI^- can significantly boost Li-ion mobility and reduce the deposition potential barrier.

https://doi.org/10.1021/acs.nanolett.5c01953
Nano Lett. 2025, 25, 10102−10113

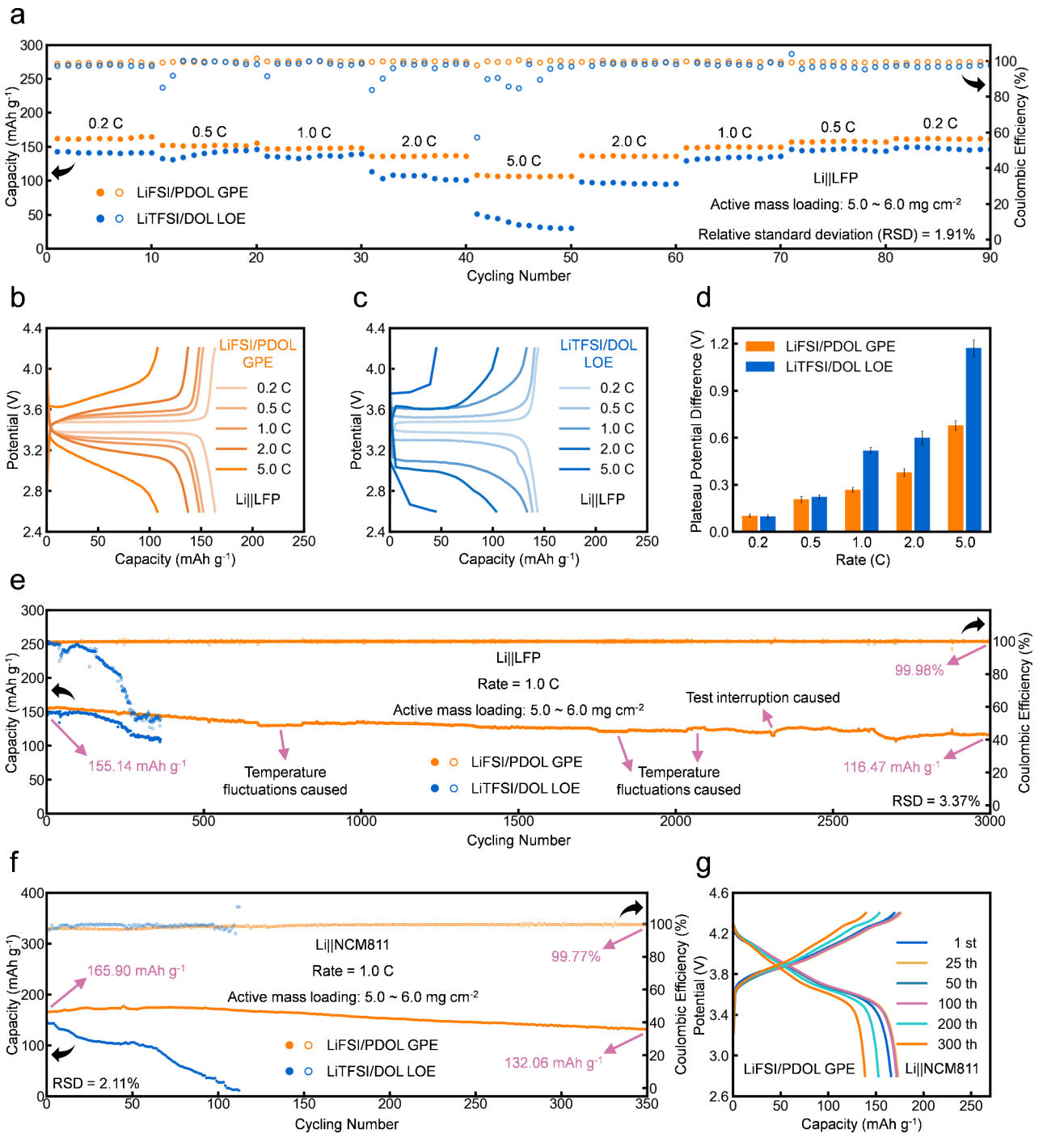

Figure 4. Electrochemical performances of LMBs. (a) Rate performances, (b, c) galvanostatic charge/discharge profiles, and (d) potential differences between charge/discharge plateaus of Li||LFP batteries assembled with LiFSI/PDOL GPE or LiTFSI/DOL LOE at various current densities. Long cycling performance of (e) Li||LFP and (f, g) Li||NCM811 batteries assembled with LiFSI/PDOL GPE or LiTFSI/DOL LOE at 1.0 C.

Ex situ X-ray photoelectron spectroscopy (XPS) analysis of cycled Li electrodes (Figure 3f–h) showed increased LiF species in the SEI layer with LiFSI/PDOL GPE. Compared to $-CF_3$, the LiF-rich SEI layer has a mechanically rigid and electronically insulated structure, homogenizing Li-ion flux distribution at the interface by guiding lateral ion diffusion, thereby suppressing dendritic lithium growth and ensuring spatially uniform plating/stripping processes.[38,40] Its exceptional mechanical robustness and chemical stability can prevent electrolyte penetration, SEI fracture, and parasitic side reactions, which are primary causes of capacity fade.[41] Additionally, the high dielectric constant and low Li-ion diffusion barriers (activation energy ≈ 0.16 eV) of LiF enable rapid Li-salt desolvation and charge transfer kinetics, and its wide bandgap and interfacial energy enhance interfacial passivation, promoting lateral Li deposition over vertical dendrite formation.[42,43]

Figure 3i and j illustrates Li deposition behaviors on Li electrodes. For LiFSI/PDOL GPE, the LiF-rich SEI layer ensures uniform Li-ion flux distribution, maintaining a smooth

https://doi.org/10.1021/acs.nanolett.5c01953
Nano Lett. 2025, 25, 10102−10113

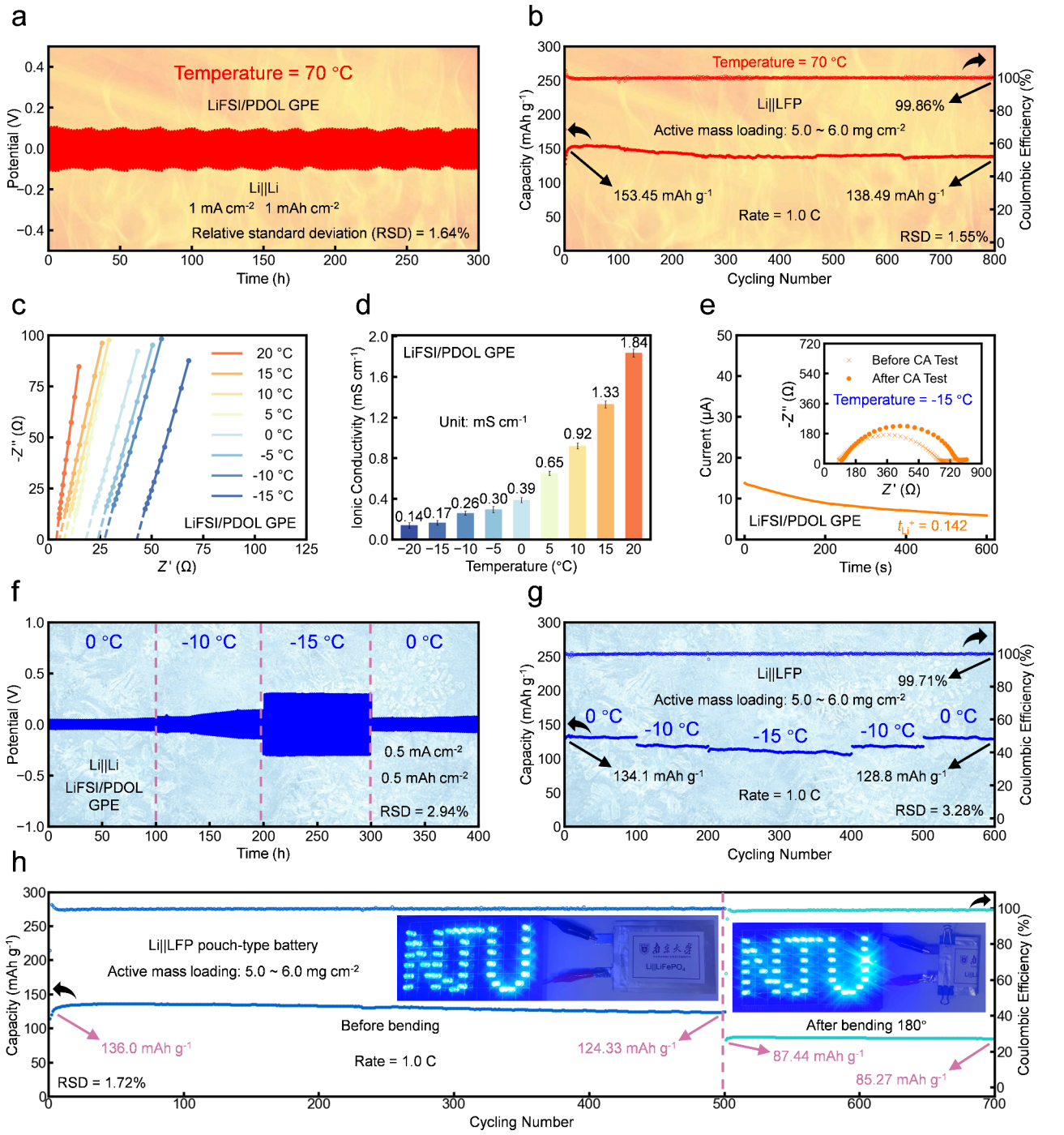

Figure 5. Temperature adaptability and bending resistance. Galvanostatic cycling stability of (a) Li||LiFSI/PDOLGPE||Li and (b) Li||LiFSI/PDOL GPE||LFP batteries at 70 °C. (c–d) Ion conductivities and (e) t_{Li}^+ of LiFSI/PDOL GPE at low temperatures. Cycling stability of (f) Li||LiFSI/PDOLGPE||Li and (g) Li||LiFSI/PDOL GPE||LFP batteries at low temperatures. (h) Cycling performance of the Li||LiFSI/PDOL GPE||LFP pouch battery under normal and 180° bending states. The insets show the pouch battery powering an LED panel under normal and 180° bending states.

surface even after long-term cycling. Conversely, LiTFSI/DOL LOE results in uneven Li nucleation, exacerbating nonuniform deposition and leading to lithium-dendrite growth, dead lithium formation, and SEI layer rupture/reconstruction, which increase the active-lithium consumption and the risk of battery short circuits.

The electrochemical stable window (ESW) of LiFSI/PDOL GPE was evaluated using linear sweep voltammetry (Figure S20), revealing its larger ESW (4.9 V) compared to LiTFSI/DOL LOE, highlighting its excellent electrochemical stability and adaptation to higher-voltage cathodic active substances (LFP, NCM811, etc.), indicating its potential for high-voltage SSLMBs.

To demonstrate its cycling performance in LMBs, Li||LFP full batteries were assembled with LiFSI/PDOL GPE or LiTFSI/DOL LOE and subjected to rate performance and long-term cycling tests. The Li||LiFSI/PDOL GPE||LFP battery exhibited higher discharge capacities at different rates

https://doi.org/10.1021/acs.nanolett.5c01953
Nano Lett. 2025, 25, 10102−10113

compared with Li||LiTFSI/DOL LOE||LFP (Figure 4a−c and Figure S21). It also showed good capacity recovery capability when switching from high rates to low rates, maintaining a noticeable charge/discharge voltage platform at 5.0 C. The superior rate performance of LiFSI/PDOL GPE was attributed to lower polarization and better reaction kinetics, as confirmed by smaller potential differences between charge/discharge plateaus. The impedance of the Li||LiFSI/PDOL GPE||LFP battery decreased initially due to SEI-layer formation and remained constant thereafter, with no significant polarization in CV curves, proving its excellent Li-ion mass-transfer kinetics (Figure S22).

Conversely, the Li||LiTFSI/DOL LOE||LFP battery exhibited a significant capacity decrease at high rates, especially at 5.0 C, where the capacity decayed to 30.3 mAh g^{-1} with minimal voltage platform and CE below 90%. The inferior rate performance of LiTFSI/DOL LOE originates from three synergistic limitations. First, sluggish Li^+ transport kinetics arises from weak solvation of LiTFSI in LOE, causing insufficient dissociation and reduced ionic conductivity under rapid ion flux demands at high rates. Second, porous SEI layers induce increased interfacial impedance and uncontrolled lithium dendrite, both of which consume active lithium and electrolyte, resulting in irreversible capacity loss and CE below 90%. Third, the low Li^+ transference number of LiTFSI/DOL LOE exacerbates a concentration polarization across electrodes at high rates, further limiting cathode capacity utilization. These factors collectively explain the rapid capacity decay and CE loss of LiTFSI/DOL LOE under high rates.

Long-term charge/discharge cycling tests revealed that the Li||LiFSI/PDOL GPE||LFP battery maintained CE above 99.5% for 3000 cycles, with a capacity retention of 75.1%, averaging a capacity attenuation of only 0.008% per cycle with a negligible voltage polarization effect (Figure 4e, f and Figure S23). Conversely, Li||LiTFSI/DOL LOE||LFP suffered significant capacity decay after 300 cycles, reducing capacity retention to 70% and achieving a CE of just 53%, owing to electrolyte corrosion and uncontrolled lithium dendrites. LiFSI/PDOL GPE also demonstrated excellent compatibility with LFP cathodes and Li metal anodes at various rates (0.2 to 5 C) and maintained long-term cycling stability (Figure S24). Especially, the Li||LiFSI/PDOL GPE||LFP battery cycled stably for 2000 cycles at 5.0 C, maintaining a CE of over 99% and an average capacity attenuation of 0.01%.

High-voltage LMBs using NCM811 were also tested. The Li||LiFSI/PDOL GPE||NCM811 battery displayed excellent cycling stability, delivering a high remaining capacity of 132.06 mAh g^{-1} after 350 cycles, with an average capacity attenuation of only 0.058% per cycle (Figure 4f, g). Conversely, Li|| LiTFSI/DOL LOE||NCM811 exhibited continuous capacity degradation at 4.4 V, decreasing to 11.8 mAh g^{-1} after 120 cycles (Figure S25). The superior cycling performance of LiFSI/PDOL GPE in Li||NCM811 batteries is attributed to better Li-ion mass-transfer kinetics, lower voltage polarization, and improved electrode−electrolyte interface contact, confirmed by smaller potential differences in charge/discharge plateaus.

A comparison of LiFSI/PDOL GPE with various reported representative GPEs (Tables S5, S6) highlights its unique combination of advantages in electrolyte thickness, ion conductivity, cycling stability, and battery lifespan (Figure S26).[6,7,9,10,12,15,16,24,25,35,44−52] Notably, LiFSI/PDOL GPE demonstrates a relatively lower production cost compared with most previous GPEs, attributable to the absence of separators and additional polymerization initiators. Furthermore, the in situ polymerization strategy significantly streamlines the preparation process complexity while well maintaining its electrochemical performance.

The stable operation of LMBs over wide temperature ranges is critical for their practical application in various climates and regions. Ensuring ion conductivity at extreme temperatures is essential for achieving excellent cycling performance. Considering the high ion conductivity of LiFSI/PDOL GPE at high temperatures tested before, Li||Li symmetric and Li||LFP full batteries were assembled to evaluate their performance at 70 °C. The Li||Li battery demonstrated exceptional cycling stability, maintaining a low voltage polarization of 100 mV over 300 h without a polarization increase or short circuits (Figure 5a). The Li||LFP battery achieved a CE of over 99.8% during 800 cycles, retaining a capacity of 138.49 mAh g^{-1} after 800 cycles at 1.0 C, with only 0.012% average attenuation per -cycle (Figure 5b).

For low-temperature adaptability, the ion conductivity and t_{Li}^+ of LiFSI/PDOL GPE were measured from 20 to −15 °C. LiFSI/PDOL GPE exhibited high ion conductivity (0.14 mS cm^{-1}) and t_{Li}^+ (0.142) at −15 °C (Figure 5d−f), indicating great potential for low-temperature applications. Cycling stability tests at low temperatures showed limited voltage polarizations (0.112, 0.246, and 0.593 mV at 0, −10, and −15 °C, respectively) and excellent stability over 800 h (Figure 5f and Figure S27). The Li||LFP battery displayed stable discharge capacities of 134.1, 120.4, and 109.8 mAh g^{-1} at 0, −10, and −15 °C, equivalent to 86.46%, 77.63%, and 70.79% of capacity at room temperature, respectively, with CE consistently above 99.5% during 800 cycles (Figure 5g and Figure S28). Furthermore, it exhibited a good capacity-recovery ability when transitioning from −15 to 0 °C.

The exceptional low-temperature electrochemical performance of LiFSI/PDOL GPE stems from multiple synergistic mechanisms. In contrast to LOE, which experiences severe viscosity increases and sluggish Li^+ diffusion at subzero temperatures, the 3D gelatinized polymer network of LiFSI/PDOL GPE maintains structural integrity and Li^+ transport pathways, retaining favorable ionic conductivity (Figure 5d) to ensure adequate Li^+ supply and effectively suppress polarization. Besides, LiFSI/PDOL GPE forms a mechanically robust and chemically homogeneous SEI layer on the electrodes, minimizing interfacial resistance growth and dendrite risks at low temperatures. These combined advantages—superior ionic transport, stabilized electrode interfaces, and dendrite suppression—collectively account for the excellent cyclic stability and reversible capability of LiFSI/PDOL GPE in cold environments.

To assess the bending resistance and wearable adaptability, soft-packed Li||LFP pouch batteries were tested. The pouch battery retained 91.42% capacity (124.33 mAh g^{-1}) after 500 cycles, keeping CE over 99% (Figure 5h). Even under the 180°-bending state, it preserved 70.33% capacity retention (87.44 mAh g^{-1}) compared to the normal state. After 200 cycles under a 180°-bending state, its capacity retention was 97.52% (0.012% average attenuation per cycle).

These results highlight the temperature adaptability and bending resistance of LiFSI/PDOL GPE and its potential for widespread use in LMBs under diverse regional and climate conditions.

https://doi.org/10.1021/acs.nanolett.5c01953
Nano Lett. 2025, 25, 10102−10113

In summary, we report an innovative GPE prepared by in situ radical-triggered ROP of DOL, without requiring additional polymerization initiators or separators. The polymerization mechanism was thoroughly explored, revealing the microscopic processes involving the break of S−F bonds in LiFSI followed by the attack of Lewis-acidic S in $\bullet(SO_2)$-$(FSO_2)N^-$ on Lewis-basic O in DOL. The resulting LiFSI/PDOL GPE exhibits high ion conductivity (1.836 mS cm^{-1}), high t_{Li}^+ (0.705), low interfacial resistance, excellent electrochemical stability, and relatively smaller production costs. Li‖LiFSI/PDOL GPE‖ symmetrical batteries maintained stable and dendrite-free cycling for over 500 h at high current density. Li‖LFP and Li‖NCM811 full batteries also displayed high CE, long-cycling lifespan, high capacity-retention capability, and excellent cycling stability. Impressively, these batteries performed outstanding cycling performance even at extreme temperatures (−15 and 70 °C) and extreme state (180° bending), highlighting their potential for deployment under harsh conditions and extreme climates. This study also underscores the simplified battery manufacturing processes represented by in situ preparation and cure of GPEs for optimizing the compositions and contact of electrode/electrolyte interfaces. Such additive-free and separator-free in situ polymerized GPEs demonstrate immense potential for widespread application in alkali metal batteries, aiming toward realization of next-generation high-performance secondary batteries.

■ ASSOCIATED CONTENT

Supporting Information

The Supporting Information is available free of charge at https://pubs.acs.org/doi/10.1021/acs.nanolett.5c01953.

Experimental details include the material and electrolyte preparation methods, characterizations, computational details, electrochemical measurements, and battery tests. Optical photographs, DFT calculation results, Nyquist diagrams, Raman spectra, SEM images, electrochemical analyses, battery test results, and performance comparisons (Figures S1−S28 and Tables S1−S7) (PDF)

■ AUTHOR INFORMATION

Corresponding Authors

Zuoxiu Tie − *State Key Laboratory of Coordination Chemistry, MOE Key Laboratory of Mesoscopic Chemistry, MOE Key Laboratory of High Performance Polymer Materials and Technology, Jiangsu Key Laboratory of Advanced Organic Materials, Suzhou Key Laboratory of Green Intelligent Manufacturing of New Energy Materials and Devices, Tianchang New Materials and Energy Technology Research Center, Institute of Green Chemistry and Engineering, School of Chemistry and Chemical Engineering, Nanjing University, Nanjing, Jiangsu 210023, P. R. China; State Key Laboratory of Solid State Microstructures, College of Engineering and Applied Sciences, Nanjing University, Nanjing, Jiangsu 210023, P. R. China; Suzhou Tierui New Energy Technology Co. Ltd., Suzhou, Jiangsu 215228, P. R. China*; Email: zxtie@nju.edu.cn

Zhong Jin − *State Key Laboratory of Coordination Chemistry, MOE Key Laboratory of Mesoscopic Chemistry, MOE Key Laboratory of High Performance Polymer Materials and Technology, Jiangsu Key Laboratory of Advanced Organic Materials, Suzhou Key Laboratory of Green Intelligent Manufacturing of New Energy Materials and Devices, Tianchang New Materials and Energy Technology Research Center, Institute of Green Chemistry and Engineering, School of Chemistry and Chemical Engineering, Nanjing University, Nanjing, Jiangsu 210023, P. R. China*; orcid.org/0000-0001-8860-8579; Email: zhongjin@nju.edu.cn

Authors

Tianyu Shen − *State Key Laboratory of Coordination Chemistry, MOE Key Laboratory of Mesoscopic Chemistry, MOE Key Laboratory of High Performance Polymer Materials and Technology, Jiangsu Key Laboratory of Advanced Organic Materials, Suzhou Key Laboratory of Green Intelligent Manufacturing of New Energy Materials and Devices, Tianchang New Materials and Energy Technology Research Center, Institute of Green Chemistry and Engineering, School of Chemistry and Chemical Engineering, Nanjing University, Nanjing, Jiangsu 210023, P. R. China; State Key Laboratory of Solid State Microstructures, College of Engineering and Applied Sciences, Nanjing University, Nanjing, Jiangsu 210023, P. R. China*

Qianchuan Yu − *State Key Laboratory of Coordination Chemistry, MOE Key Laboratory of Mesoscopic Chemistry, MOE Key Laboratory of High Performance Polymer Materials and Technology, Jiangsu Key Laboratory of Advanced Organic Materials, Suzhou Key Laboratory of Green Intelligent Manufacturing of New Energy Materials and Devices, Tianchang New Materials and Energy Technology Research Center, Institute of Green Chemistry and Engineering, School of Chemistry and Chemical Engineering, Nanjing University, Nanjing, Jiangsu 210023, P. R. China*

Jie Wei − *State Key Laboratory of Coordination Chemistry, MOE Key Laboratory of Mesoscopic Chemistry, MOE Key Laboratory of High Performance Polymer Materials and Technology, Jiangsu Key Laboratory of Advanced Organic Materials, Suzhou Key Laboratory of Green Intelligent Manufacturing of New Energy Materials and Devices, Tianchang New Materials and Energy Technology Research Center, Institute of Green Chemistry and Engineering, School of Chemistry and Chemical Engineering, Nanjing University, Nanjing, Jiangsu 210023, P. R. China*

Yaoda Wang − *State Key Laboratory of Coordination Chemistry, MOE Key Laboratory of Mesoscopic Chemistry, MOE Key Laboratory of High Performance Polymer Materials and Technology, Jiangsu Key Laboratory of Advanced Organic Materials, Suzhou Key Laboratory of Green Intelligent Manufacturing of New Energy Materials and Devices, Tianchang New Materials and Energy Technology Research Center, Institute of Green Chemistry and Engineering, School of Chemistry and Chemical Engineering, Nanjing University, Nanjing, Jiangsu 210023, P. R. China*

Huaizhu Wang − *State Key Laboratory of Coordination Chemistry, MOE Key Laboratory of Mesoscopic Chemistry, MOE Key Laboratory of High Performance Polymer Materials and Technology, Jiangsu Key Laboratory of Advanced Organic Materials, Suzhou Key Laboratory of Green Intelligent Manufacturing of New Energy Materials and Devices, Tianchang New Materials and Energy Technology Research Center, Institute of Green Chemistry and Engineering, School of Chemistry and Chemical*

https://doi.org/10.1021/acs.nanolett.5c01953
Nano Lett. 2025, 25, 10102−10113

Engineering, Nanjing University, Nanjing, Jiangsu 210023, P. R. China

Zhenchao Li − *State Key Laboratory of Coordination Chemistry, MOE Key Laboratory of Mesoscopic Chemistry, MOE Key Laboratory of High Performance Polymer Materials and Technology, Jiangsu Key Laboratory of Advanced Organic Materials, Suzhou Key Laboratory of Green Intelligent Manufacturing of New Energy Materials and Devices, Tianchang New Materials and Energy Technology Research Center, Institute of Green Chemistry and Engineering, School of Chemistry and Chemical Engineering, Nanjing University, Nanjing, Jiangsu 210023, P. R. China*

Xingkai Ma − *State Key Laboratory of Coordination Chemistry, MOE Key Laboratory of Mesoscopic Chemistry, MOE Key Laboratory of High Performance Polymer Materials and Technology, Jiangsu Key Laboratory of Advanced Organic Materials, Suzhou Key Laboratory of Green Intelligent Manufacturing of New Energy Materials and Devices, Tianchang New Materials and Energy Technology Research Center, Institute of Green Chemistry and Engineering, School of Chemistry and Chemical Engineering, Nanjing University, Nanjing, Jiangsu 210023, P. R. China*

Jingjie Sun − *State Key Laboratory of Coordination Chemistry, MOE Key Laboratory of Mesoscopic Chemistry, MOE Key Laboratory of High Performance Polymer Materials and Technology, Jiangsu Key Laboratory of Advanced Organic Materials, Suzhou Key Laboratory of Green Intelligent Manufacturing of New Energy Materials and Devices, Tianchang New Materials and Energy Technology Research Center, Institute of Green Chemistry and Engineering, School of Chemistry and Chemical Engineering, Nanjing University, Nanjing, Jiangsu 210023, P. R. China*

Jing Ma − *State Key Laboratory of Coordination Chemistry, MOE Key Laboratory of Mesoscopic Chemistry, MOE Key Laboratory of High Performance Polymer Materials and Technology, Jiangsu Key Laboratory of Advanced Organic Materials, Suzhou Key Laboratory of Green Intelligent Manufacturing of New Energy Materials and Devices, Tianchang New Materials and Energy Technology Research Center, Institute of Green Chemistry and Engineering, School of Chemistry and Chemical Engineering, Nanjing University, Nanjing, Jiangsu 210023, P. R. China;* orcid.org/0000-0001-5848-9775

Complete contact information is available at: https://pubs.acs.org/10.1021/acs.nanolett.5c01953

Notes

The authors declare no competing financial interest.

■ ACKNOWLEDGMENTS

The authors are grateful to the funding supports from the National Natural Science Foundation of China (Nos. 22479074, 22475096), the Equipment Pre-Research and Ministry of Education Joint Fund General Project (No. 8091B02052407), the Natural Science Foundation of Jiangsu Province (Nos. BK20240400, BK20241236), the Jiangsu Province Science and Technology Major Project (No. BG2024013), the Jiangsu Province Scientific and Technological Achievements Transformation Special Fund (No. BA2023037), the Jiangsu Province Academic Degree and Postgraduate Education Reform Project (No. JGKT24_C001), the Suzhou City Key Core Technology Open Competition Project (No. SYG2024122), the Open Research Fund of Suzhou Laboratory (No. SZLAB-1308-2024-TS005), the Suzhou City Gusu Leading Talent Program of Scientific and Technological Innovation and Entrepreneurship in Wujiang District (No. ZXL2021273), and the Chenzhou National Sustainable Development Agenda Innovation Demonstration Zone Provincial Special Project (No. 2023sfq11).

■ REFERENCES

(1) Liu, K.; Lin, Y.; Miller, J. D.; Liu, J.; Wang, X. Study of sucrose based room temperature solid polymer electrolyte for lithium sulfur battery. *J. Electrochem. Soc.* **2017**, *164*, A447.

(2) Miao, R.; Yang, J.; Feng, X.; Jia, H.; Wang, J.; Nuli, Y. Novel dual-salts electrolyte solution for dendrite-free lithium-metal based rechargeable batteries with high cycle reversibility. *J. Power Sources* **2014**, *271*, 291−297.

(3) Ye, Q.; Zheng, P.; Ao, X.; Yao, D.; Lei, Z.; Deng, Y.; Wang, C. Novel multi-block conductive binder with polybutadiene for Si anodes in lithium-ion batteries. *Electrochim. Acta* **2019**, *315*, 58−66.

(4) Sun, P.; Chen, J.; Huang, Y.; Tian, J.-H.; Li, S.; Wang, G.; Zhang, Q.; Tian, Z.; Zhang, L. High-strength agarose gel electrolyte enables long-endurance wearable Al-air batteries with greatly suppressed self-corrosion. *Energy Storage Materials* **2021**, *34*, 427−435.

(5) Goodenough, J. B.; Kim, Y. Challenges for rechargeable Li batteries. *Chem. Mater.* **2010**, *22* (3), 587−603.

(6) Zhao, Q.; Liu, X.; Stalin, S.; Khan, K.; Archer, L. A. Solid-state polymer electrolytes with in-built fast interfacial transport for secondary lithium batteries. *Nature Energy* **2019**, *4*, 365−373.

(7) Liu, F.-Q.; Wang, W.-P.; Yin, Y.-X.; Zhang, S.-F.; Shi, J.-L.; Wang, L.; Zhang, X.-D.; Zheng, Y.; Zhou, J.-J.; Li, L.; Guo, Y.-G. Upgrading traditional liquid electrolyte via in situ gelation for future lithium metal batteries. *Science Advances* **2018**, *4* (10), No. eaat5383.

(8) Xu, Y.; Wang, K.; An, Y.; Liu, W.; Li, C.; Zheng, S.; Zhang, X.; Wang, L.; Sun, X.; Ma, Y. Rapid ion transport induced by the enhanced interaction in composite polymer electrolyte for all-solid-state lithium-metal batteries. *J. Phys. Chem. Lett.* **2021**, *12* (43), 10603−10609.

(9) Wang, Y.; Xu, R.; Xiao, B.; Lv, D.; Peng, Y.; Zheng, Y.; Shen, Y.; Chai, J.; Lei, X.; Luo, S.; Wang, X.; Liang, X.; Feng, J.; Liu, Z. A poly(1,3-dioxolane) based deep-eutectic polymer electrolyte for high performance ambient polymer lithium battery. *Materials Today Physics* **2022**, *22*, 100620.

(10) Li, W.; Gao, J.; Tian, H.; Li, X.; He, S.; Li, J.; Wang, W.; Li, L.; Li, H.; Qiu, J.; Zhou, W. SnF_2-catalyzed formation of polymerized dioxolane as solid electrolyte and its thermal decomposition behavior. *Angew. Chem., Int. Ed.* **2022**, *61* (6), No. e202114805.

(11) Liu, B.; Zhang, J.-G.; Xu, W. Advancing lithium metal batteries. *Joule* **2018**, *2*, 833−845.

(12) Yan, W.; Wei, J.; Chen, T.; Duan, L.; Wang, L.; Xue, X.; Chen, R.; Kong, W.; Lin, H.; Li, C.; Jin, Z. Superstretchable, thermostable and ultrahigh-loading lithium-sulfur batteries based on nanostructural gel cathodes and gel electrolytes. *Nano Energy* **2021**, *80*, 105510.

(13) Lin, Y.; Li, J.; Liu, K.; Liu, Y.; Liu, J.; Wang, X. Unique starch polymer electrolyte for high capacity all-solid-state lithium sulfur battery. *Green Chem.* **2016**, *18*, 3796−3803.

(14) Li, J.; Daniel, C.; Wood, D. Materials processing for lithium-ion batteries. *J. Power Sources* **2011**, *196* (5), 2452−2460.

(15) Chen, D.; Zhu, M.; Kang, P.; Zhu, T.; Yuan, H.; Lan, J.; Yang, X.; Sui, G. Self-enhancing gel polymer electrolyte by in situ construction for enabling safe lithium metal battery. *Advanced Science* **2022**, *9* (4), 2103663.

(16) Wan, Z.; Lei, D.; Yang, W.; Liu, C.; Shi, K.; Hao, X.; Shen, L.; Lv, W.; Li, B.; Yang, Q.-H.; Kang, F.; He, Y.-B. Low resistance-integrated all-solid-state battery achieved by $Li_7La_3Zr_2O_{12}$ nanowire

upgrading Polyethylene oxide (PEO) composite electrolyte and PEO cathode binder. *Adv. Funct. Mater.* **2019**, *29* (1), 1805301.
(17) Xu, K. Electrolytes and interphases in Li-ion batteries and beyond. *Chem. Rev.* **2014**, *114* (23), 11503−11618.
(18) Scrosati, B.; Garche, J. Lithium batteries: Status, prospects and future. *J. Power Sources* **2010**, *195* (9), 2419−2430.
(19) Murata, K. An overview of the research and development of solid polymer electrolyte batteries. *Electrochim. Acta* **1995**, *40* (13−14), 2177−2184.
(20) Sekhon, S. S.; Singh, H. P. Proton conduction in polymer gel electrolytes containing chloroacetic acids. *Solid State Ionics* **2004**, *175* (1−4), 545−548.
(21) Ma, L.; Chen, S.; Li, X.; Chen, A.; Dong, B.; Zhi, C. Liquid-free all-solid-state zinc batteries and encapsulation-free flexible batteries enabled by in situ constructed polymer electrolyte. *Angew. Chem., Int. Ed.* **2020**, *59* (52), 23836−23844.
(22) Croce, F.; D'Epifanio, A.; Hassoun, J.; Reale, P.; Scrosati, B. Advanced electrolyte and electrode materials for lithium polymer batteries. *J. Power Sources* **2003**, *119*−*121*, 399−402.
(23) Fauteux, D.; Massucco, A.; McLin, M.; Van Buren, M.; Shi, J. Lithium polymer electrolyte rechargeable battery. *Electrochim. Acta* **1995**, *40* (13−14), 2185−2190.
(24) Tao, J.; Wang, D.; Yang, Y.; Li, J.; Huang, Z.; Mathur, S.; Hong, Z.; Lin, Y. Swallowing lithium dendrites in all-solid-state battery by lithiation with silicon nanoparticles. *Advanced Science* **2022**, *9* (4), 2103786.
(25) Li, W.; Chen, L.; Sun, Y.; Wang, C.; Wang, Y.; Xia, Y. All-solid-state secondary lithium battery using solid polymer electrolyte and anthraquinone cathode. *Solid State Ionics* **2017**, *300*, 114−119.
(26) Song, J. Y.; Wang, Y. Y.; Wan, C. C. Review of gel-type polymer electrolytes for lithium-ion batteries. *J. Power Sources* **1999**, *77* (2), 183−197.
(27) Choudhury, S.; Tu, Z.; Nijamudheen, A.; Zachman, M. J.; Stalin, S.; Deng, Y.; Zhao, Q.; Vu, D.; Kourkoutis, L. F.; Mendoza-Cortes, J. L.; Archer, L. A. Stabilizing polymer electrolytes in high-voltage lithium batteries. *Nat. Commun.* **2019**, *10*, 3091.
(28) Tian, L.; Xiong, L.; Chen, X.; Guo, H.; Zhang, H.; Chen, X. Enhanced electrochemical properties of gel polymer electrolyte with hybrid copolymer of organic palygorskite and methyl methacrylate. *Materials* **2018**, *11* (10), 1814.
(29) Zhang, M. Y.; Li, M. X.; Chang, Z.; Wang, Y. F.; Gao, J.; Zhu, Y. S.; Wu, Y. P.; Huang, W. A sandwich PVDF/HEC/PVDF gel polymer electrolyte for lithium ion battery. *Electrochim. Acta* **2017**, *245*, 752−759.
(30) Camacho-Forero, L. E.; Balbuena, P. B. Effects of charged interfaces on electrolyte decomposition at the lithium metal anode. *J. Power Sources* **2020**, *472*, 228449.
(31) Ma, Q.; Yue, J.; Fan, M.; Tan, S.-J.; Zhang, J.; Wang, W.-P.; Liu, Y.; Tian, Y.-F.; Xu, Q.; Yin, Y.-X.; You, Y.; Luo, A.; Xin, S.; Wu, X.-W.; Guo, Y.-G. Formulating the electrolyte towards high-energy and safe rechargeable lithium-metal batteries. *Angew. Chem., Int. Ed.* **2021**, *60* (30), 16554−16560.
(32) Zhao, C.-Z.; Zhao, Q.; Liu, X.; Zheng, J.; Stalin, S.; Zhang, Q.; Archer, L. A. Rechargeable lithium metal batteries with an in-built solid-state polymer electrolyte and a high voltage/loading Ni-rich layered cathode. *Adv. Mater.* **2020**, *32* (12), 1905629.
(33) Liu, Q.; Cai, B.; Li, S.; Yu, Q.; Lv, F.; Kang, F.; Wang, Q.; Li, B. Long-cycling and safe lithium metal batteries enabled by the synergetic strategy of ex situ anodic pretreatment and an in-built gel polymer electrolyte. *Journal of Materials Chemistry A* **2020**, *8*, 7197−7204.
(34) Okada, M.; Yamashita, Y.; Ishii, Y. Polymerization of 1,3-dioxolane. *Makromol. Chem.* **1964**, *80* (1), 196−207.
(35) Li, M.; Yang, J.; Shi, Y.; Chen, Z.; Bai, P.; Su, H.; Xiong, P.; Cheng, M.; Zhao, J.; Xu, Y. Soluble organic cathodes enable long cycle life, high rate, and wide-temperature lithium-ion batteries. *Adv. Mater.* **2022**, *34* (5), 2107226.
(36) Hou, T.; Qian, Y.; Li, D.; Xu, B.; Huang, Z.; Liu, X.; Wang, H.; Jiang, B.; Xu, H.; Huang, Y. Electronegativity-induced single-ion conducting polymer electrolyte for solid-state lithium batteries. *Energy & Environmental Materials* **2023**, *6* (4), No. e12428.
(37) Li, X.-Y.; Feng, S.; Zhao, C.-X.; Cheng, Q.; Chen, Z.-X.; Sun, S.-Y.; Chen, X.; Zhang, X.-Q.; Li, B.-Q.; Huang, J.-Q.; Zhang, Q. Regulating lithium salt to inhibit surface gelation on an electrocatalyst for high-energy-density lithium−sulfur batteries. *J. Am. Chem. Soc.* **2022**, *144* (32), 14638−14646.
(38) Huang, J.; Hollenkamp, A. F. Thermal behavior of ionic liquids containing the FSI anion and the Li^+ cation. *J. Phys. Chem. C* **2010**, *114* (49), 21840−21847.
(39) Aurbach, D.; Gofer, Y.; Langzam, J. The correlation between surface chemistry, surface morphology, and cycling efficiency of lithium electrodes in a few polar aprotic systems. *J. Electrochem. Soc.* **1989**, *136*, 3198−3205.
(40) Qian, J.; Xu, W.; Bhattacharya, P.; Engelhard, M.; Henderson, W. A.; Zhang, Y.; Zhang, J.-G. Dendrite-free Li deposition using trace-amounts of water as an electrolyte additive. *Nano Energy* **2015**, *15*, 135−144.
(41) Liang, W.; Zhou, X.; Zhang, B.; Zhao, Z.; Song, X.; Chen, K.; Wang, L.; Ma, Z.; Liu, J. The versatile establishment of charge storage in polymer solid electrolyte with enhanced charge transfer for LiF-rich SEI generation in lithium metal batteries. *Angew. Chem., Int. Ed.* **2024**, *63* (18), No. e202320149.
(42) Zhang, J.; Yue, X.; Wu, Z.; Chen, Y.; Bai, Y.; Sun, K.; Wang, Z.; Liang, Z. A LiF-rich solid electrolyte interphase in a routine carbonate electrolyte by tuning the interfacial chemistry behavior of $LiPF_6$ for stable Li metal anodes. *Nano Lett.* **2023**, *23* (20), 9609−9617.
(43) Shen, H.; Yu, T.; Tang, P.; Yang, H.; Tan, J.; Bai, S.; Li, F. Spatially selective solvation structure by electronegative micro-arrays for stable lithium-metal anode interface. *Adv. Mater.* **2024**, *36* (11), 2306553.
(44) Yu, J.; Zhou, G.; Li, Y.; Wang, Y.; Chen, D.; Ciucci, F. Improving Room-Temperature Li-Metal Battery Performance by In Situ Creation of Fast Li^+ Transport Pathways in a Polymer-Ceramic Electrolyte. *Small* **2023**, *19* (39), 2302691.
(45) Wang, Y.; Chen, S.; Li, Z.; Peng, C.; Li, Y.; Feng, W. In-situ generation of fluorinated polycarbonate copolymer solid electrolytes for high-voltage Li-metal batteries. *Energy Storage Materials* **2022**, *45*, 474−483.
(46) Ren, Z.; Li, J.; Cai, M.; Yin, R.; Liang, J.; Zhang, Q.; He, C.; Jiang, X.; Ren, X. An in situ formed copolymer electrolyte with high ionic conductivity and high lithium-ion transference-number for dendrite-free solid-state lithium metal batteries. *Journal of Materials Chemistry A* **2023**, *11*, 1966−1977.
(47) Xu, H.; Mi, J.; Ma, J.; Han, Z.; Lv, S.; Chen, L.; Zhang, J.; Yang, K.; Li, B.; Li, Y.; An, X.; Ma, Y.; Guo, S.; Su, H.; Shi, P.; Liu, M.; Kang, F.; He, Y.-B. Mg^{2+} initiated in situ polymerization of dioxolane enabling stable interfaces in solid-state lithium metal batteries. *Energy Environ. Sci.* **2025**, *18*, 4231.
(48) Li, T.; Chen, K.; Yang, B.; Li, K.; Li, B.; He, M.; Yang, L.; Hu, A.; Long, J. In situ polymerization of 1,3-dioxolane and formation of fluorine/boron-rich interfaces enabled by film-forming additives for long-life lithium metal batteries. *Chemical Science* **2024**, *15*, 12108−12117.
(49) He, C.; Ying, H.; Cai, L.; Chen, H.; Xu, Z.; Liu, S.; Huang, P.; Zhang, H.; Song, W.; Zhang, J.; Shi, L.; Gao, W.; Li, D.; Han, W.-Q. Tailoring stable peo-based electrolyte/electrodes interfaces via molecular coordination regulating enables 4.5 V solid-state lithium metal batteries. *Adv. Funct. Mater.* **2024**, *34* (51), 2410350.
(50) Liu, Q.; Dan, Y.; Niu, Y.; Lv, Y.; Li, G. A highly compatible deep eutectic solvent-based poly(ethylene) oxide polymer electrolyte to enable the stable operation of 4.5 V lithium metal batteries. *Small* **2025**, *21* (2), 2408944.
(51) Jiang, X.; Liu, Z.; Liu, W.; Yu, D.; Zhang, J.; Wang, X.; Zhang, Y.; Zhang, S. Physical ionogels with only 2 wt% gelators as efficient quasi-solid-state electrolytes for lithium batteries. *Matter* **2024**, *7* (4), 1558−1574.
(52) Min, W.; Li, L.; Wang, M.; Ma, S.; Feng, H.; Wang, W.; Ding, H.; Cheng, T.; Li, Z.; Saito, T.; Yang, H.; Cao, P.-F. Mastering the

https://doi.org/10.1021/acs.nanolett.5c01953
Nano Lett. 2025, 25, 10102−10113

copolymerization behavior of ethyl cyanoacrylate as gel polymer electrolyte for lithium-metal battery application. *Angew. Chem., Int. Ed.* **2025**, *64* (13), No. e202422510.

https://doi.org/10.1021/acs.nanolett.5c01953
Nano Lett. 2025, 25, 10102−10113